Controlled Synthesis of Gold Nanobelts and Nanocombs in Aqueous Mixed Surfactant Solutions

Nana Zhao, Yang Wei, Nijuan Sun, Qian Chen, Jingwei Bai, Longping Zhou, Yao Qin, Meixian Li, and Limin Qi*

Beijing National Laboratory for Molecular Sciences, State Key Laboratory for Structural Chemistry of Unstable and Stable Species, College of Chemistry, Peking University, Beijing 100871, P. R. China

Received September 13, 2007. In Final Form: November 6, 2007

Well-defined gold nanobelts as well as unique gold nanocombs made of nanobelts were readily synthesized by the reduction of $HAuCl_4$ with ascorbic acid in aqueous mixed solutions of the cationic surfactant cetyltrimethylammonium bromide (CTAB) and the anionic surfactant sodium dodecylsulfonate (SDSn). Single-crystalline gold nanobelts grown along the <110> and <211> directions were prepared in mixed CTAB−SDSn solutions at 4 and 27 °C, respectively. Furthermore, single-crystalline gold nanocombs consisting of a <110>-oriented stem nanobelt and numerous <211>-oriented nanobelts grown perpendicularly on one side of the stem were fabricated by a two-step process with temperature changing from 4 to 27 °C. It was proposed that the mixed cationic−anionic surfactants exerted a subtle control on the growth of gold nanocrystals in solution due to the cooperative effect of mixed surfactants. This synthetic strategy may open a new route for the mild fabrication and hierarchical assembly of metal nanobelts in solution. The obtained gold nanobelts showed good electrocatalytic activity toward the oxidation of methanol in alkaline solution; in particular, the electrode modified with the nanobelts obtained at 27 °C exhibited an electrocatalytic activity considerably higher than normal polycrystalline gold electrode. Moreover, the gold nanobelts were used as the surface-enhanced Raman scattering (SERS) substrate for detecting the enhanced Raman spectra of *p*-aminothiophenol (PATP) molecules, and the gold nanobelts obtained at 4 °C exhibited an unusual larger enhancement of the b_2 modes relative to the a_1 modes for the adsorbed PATP molecules.

Introduction

Gold nanostructures have been the focus of intense research owing to their fascinating optical, electronic, and chemical properties and promising applications in nanoelectronics, biomedicine, sensing, and catalysis.[1] Since the shape of gold nanostructures considerably influences their intrinsic properties and relevant applications, great efforts have been devoted to the morphology-controlled synthesis of gold nanostructures in the past few years.[2] In particular, a variety of wet chemical methods have been developed to fabricate gold nanoparticles with various shapes such as rods,[3] wires,[4] plates,[4,5] prisms,[6] cubes,[7] polyhedra,[8] and branched particles.[9] As a new family of one-dimensional (1D) nanostructures with unique properties, inorganic nanobelts have attracted much attention since the first report of ZnO nanobelts.[10] However, chemical synthesis of gold nanobelts has not been realized until recently when a sonochemical method was introduced.[11] It is worthwhile to explore facile solution routes to gold nanobelts with controlled growth direction. Furthermore, it remains a great challenge to fabricate hierarchical gold architectures made of nanobelts, which is a crucial step toward integrating gold nanobelts into complex functional nanosystems. It is noted that while the cationic surfactant cetyltrimethylammonium bromide (CTAB) has been frequently used as capping agent for the controlled synthesis of gold nanoparticles with multiple shapes in aqueous solutions,[3,12] the anionic surfactant sodium dodecylsulfonate (SDSn) was once employed to prepare tadpole-shaped gold nanoparticles.[13] Our recent work showed that aqueous cationic/anionic surfactant mixtures were very effective in morphological control of PbS nanocrystals,[14] which led us to further explore the use of mixed CTAB−SDSn solutions for the shape-controlled synthesis of gold nanostructures.

In recent years, electrooxidation of methanol has been commonly used to evaluate the catalytic activity of gold

* To whom correspondence should be addressed. E-mail: liminqi@pku.edu.cn.

(1) (a) Daniel, M.-C.; Astruc, D. *Chem. Rev.* **2004**, *104*, 293. (b) Hu, M.; Chen, J.; Li, Z.-Y.; Au, L.; Hartland, G. V.; Li, X.; Marguez, M.; Xia, Y. *Chem. Soc. Rev.* **2006**, *35*, 1084.

(2) (a) Wiley, B.; Sun, Y.; Chen, J.; Cang, H.; Li, Z.-Y.; Li, X.; Xia, Y. *MRS Bull.* **2005**, *30*, 356. (b) Chen, J.; Wiley, B. J.; Xia, Y. *Langmuir* **2007**, *23*, 4120. (c) Murphy, C. J.; Sau, T. K.; Gole, A. M.; Orendorff, C. J.; Gao, J.; Gou, L.; Hunyadi, S. E.; Li, T. *J. Phys. Chem. B* **2005**, *109*, 13857. (d) Murphy, C. J.; Gole, A. M.; Hungyadi, S. E.; Orendorff, C. J. *Inorg. Chem.* **2006**, *45*, 7544.

(3) (a) Jana, N.; Gearheart, L.; Murphy, C. *J. Phys. Chem. B* **2001**, *105*, 4065. (b) Kim, F.; Song, J. H.; Yang, P. *J. Am. Chem. Soc.* **2002**, *124*, 14316. (c) Kou, X.; Zhang, S.; Tsung, C.-K.; Yang, Z.; Yeung, M. H.; Stucky, G. D.; Sun, L.; Wang, J.; Yan, C. *Chem. Eur. J.* **2007**, *13*, 2929. (d) Iqbal, M.; Chung, Y. I.; Tae, G. Y. *J. Mater. Chem.* **2007**, *17*, 335.

(4) (a) Kim, J.-U.; Cha, S.-H.; Shin, K.; Jho, J. Y.; Lee, J.-C. *Adv. Mater.* **2004**, *16*, 459. (b) Vasilev, K.; Zhu, T.; Wilms, M.; Gillies, G.; Lieberwirth, I.; Mittler, S.; Knoll, W.; Kreiter, M. *Langmuir* **2005**, *21*, 12399. (c) Halder, A.; Ravishankar, N. *Adv. Mater.* **2007**, *19*, 1854.

(5) (a) Sun, X.; Dong, S.; Wang, E. *Angew. Chem., Int. Ed.* **2004**, *43*, 6360. (b) Shao, Y.; Jin, Y.; Dong, S. *Chem. Commun.* **2004**, 1104.

(6) (a) Millstone, J. E.; Park, S.; Shuford, K. L.; Qin, L.; Schatz, G. C.; Mirkin, C. A. *J. Am. Chem. Soc.* **2005**, *127*, 5312. (b) Ha, T. W.; Koo, H. J.; Chung, B. H. *J. Phys. Chem. C* **2007**, *111*, 1123.

(7) Jin, R.; Egusa, S.; Scherer, N. F. *J. Am. Chem. Soc.* **2004**, *126*, 9900.

(8) (a) Kim, F.; Connor, S.; Song, H.; Kuykendall, T.; Yang, P. *Angew. Chem., Int. Ed.* **2004**, *43*, 3673. (b) Seo, D.; Park, J. C.; Song, H. *J. Am. Chem. Soc.* **2006**, *128*, 14863. (c) Li, C.; Shuford, K. L.; Park, Q. H.; Cai, W.; Li, Y.; Lee, E. J.; Cho, S. O. *Angew. Chem., Int. Ed.* **2007**, *46*, 3264.

(9) (a) Chen, S.; Wang, Z. L.; Ballato, J.; Foulger, S. H.; Carroll, D. L. *J. Am. Chem. Soc.* **2003**, *125*, 16186. (b) Hao, E.; Bailey, R. C.; Schatz, G. C.; Hupp, J. T.; Li, S. *Nano Lett.* **2004**, *4*, 327. (c) Chen, H. M.; Hsin, C. F.; Liu, R.-S.; Lee, J.-F.; Jang, L.-Y. *J. Phys. Chem. C* **2007**, *111*, 5909. (d) Krichevski, O.; Markovich, G. *Langmuir* **2007**, *23*, 1496. (e) Jena, B. K.; Raj, C. R. *Langmuir* **2007**, *23*, 4064. (f) Li, Z.; Ravaine, V.; Ravaine, S. R.; Garrigue, P.; Kuhn, A. *Adv. Func. Mater.* **2007**, *17*, 618. (g) Xie, J.; Lee, J. Y.; Wang, D. I. C. *Chem. Mater.* **2007**, *19*, 2823. (h) Lu, G.; Li, C.; Shi, G. *Chem. Mater.* **2007**, *19*, 3433.

(10) Pan, Z. W.; Dai, Z. R.; Wang, Z. L. *Science* **2001**, *291*, 1947.

(11) Zhang, J.; Du, J.; Han, B.; Liu, Z.; Jiang, T.; Zhang, Z. *Angew. Chem., Int. Ed.* **2006**, *45*, 1116.

(12) Sau, T.; Murphy, C. J. *J. Am. Chem. Soc.* **2004**, *126*, 8648.

(13) Hu, J.; Zhang, Y.; Liu, B.; Liu, J.; Zhou, H.; Xu, Y.; Jiang, Y.; Yang, Z.; Tian, Z.-Q. *J. Am. Chem. Soc.* **2004**, *126*, 9470.

(14) Zhao, N.; Qi, L. *Adv. Mater.* **2006**, *18*, 359.

10.1021/la702848x CCC: $40.75
Published on Web 01/04/2008

nanomaterials.[15] Au is usually considered as a poor catalyst toward methanol oxidation, but a great advantage of Au as the catalyst is that poisoning intermediates are not formed.[16] It has been reported that gold nanoparticles can exhibit high electrocatalytic activity for methanol oxidation, and the catalytic property largely depends on their size and shape.[9e,15,17,18] On the other hand, gold represents a good substrate for surface-enhanced Raman scattering (SERS), which is a powerful method for research and application in the fields of analytical chemistry, biochemistry, and catalysis.[19] Various gold nanostructures have been used as the SERS substrates,[9h,20] and it has been found that the SERS enhancement ability is largely dependent on the size and shape of the nanoparticles as well as the assembled structure.[21]

Herein, we report the mixed surfactants-controlled synthesis of single-crystalline gold nanobelts elongated along the <110> and <211> directions and unique gold nanocombs with <211>-oriented nanobelts grown perpendicularly on one side of the <110>-oriented nanobelt. Moreover, the electrocatalytic activity toward the oxidation of methanol and the SERS sensitivity for detecting *p*-aminothiophenol molecules have been investigated to demonstrate potential applications of the obtained gold nanobelts.

Experimental Section

Materials. Cetyltrimethylammonium bromide (CTAB, 99%) was obtained from Jining Chemical Engineering Research Institute of China. Sodium dodecylsulfonate (SDSn, 97%) was obtained from Shantou Guanghua Chemical Co. of China. Ascorbic acid (99.7%) and hydrochloroauric acid trihydrate ($HAuCl_4 \cdot 3H_2O$, 99.9%) were obtained from Beijing Chemical Reagents Co. *p*-Aminothiophenol (PATP) was purchased from Alfa Aesar. They were all used as received. All other chemicals were of analytical grade. The water used was deionized.

Synthesis of Gold Nanobelts and Nanocombs. The synthesis of gold nanobelt-based nanostructures was simply achieved by the reduction of $HAuCl_4$ with ascorbic acid in aqueous mixed CTAB−SDSn solutions. In a typical synthesis, 3.45 mL of water, 0.65 mL of 0.05 M CTAB, 0.50 mL of 0.01 M SDSn, and 0.10 mL of 0.01 M $HAuCl_4$ were first mixed at room temperature to give a yellowish solution. Then, 0.30 mL of 0.1 M ascorbic acid was mixed with the solution at either 4 or 27 °C, which was kept at this temperature under static conditions for ∼12 h, leading to formation of Au nanobelts. For the preparation of Au nanocombs, the mixed solution was first kept at 4 °C for 0.5 h and subsequently at 27 °C for ∼12 h. The samples were collected by centrifugation and washed three times with deionized water.

Characterization. The products were characterized by scanning electron microscopy (SEM, Hitachi S4800, 15 kV), transmission electron microscopy (TEM, JEOL JEM-200CX, 160 kV), high-resolution TEM (HRTEM, FEI Tecnai F30, 300 kV), X-ray diffraction (XRD, Rigaku Dmax-2000, Ni-filtered Cu Kα radiation), and UV−vis spectroscopy (Perkin-Elmer Lambda 35). For the XRD measurements, the gold product was dispersed in water and several drops of the suspension were dropped on a clean glass slide, followed by drying naturally in the air. For the TEM and SEM measurements, the suspension was dropped onto a Formvar-covered copper grid and a silicon wafer, respectively, followed by drying naturally.

A CHI 660A electrochemical workstation (Shanghai CH Instruments, China) with a conventional three-electrode cell was used to perform electrochemical measurements. The working electrode was a glassy carbon electrode with a diameter of 4 mm. A KCl-saturated calomel electrode (SCE) was used as the reference electrode and a platinum electrode as the auxiliary electrode. All electrochemical experiments were conducted at ambient temperature (25 ± 2 °C). For the preparation of gold nanobelts-modified electrodes, the prepared gold nanobelts were dispersed in acetone to obtain a uniform suspension of ∼3 mg mL^{-1} by sonication. Glassy carbon (GC) electrodes were first polished with 0.05 μm alumina slurry and then washed ultrasonically in triply distilled water and ethanol for a few minutes. The GC electrodes were coated by casting 30 μL of the above gold nanobelts suspension and dried under an infrared lamp. Finally, 1 wt % Nafion solution in alcohol was cast on the surface of the sample and dried naturally in the air.

Raman measurements were made with a Renishaw System 1000 Raman imaging microscope (Renishaw plc, U.K.) equipped with a 25 mW (632.8 nm) He−Ne laser (model 127-25RP, Spectra-Physics, USA) and a Peltier-cooled CCD detector (576 pixels × 384 pixels). A 50× objective (NA = 0.80) mounted on an Olympus BH-2 microscope was used to focus the laser onto a spot approximately 1 μm in diameter and collect the back-scattered light from the sample. For the preparation of SERS samples, the *p*-aminothiophenol (PATP) molecules were assembled on the surface of various gold products by immersing in 5 mM PATP solution for 12 h to ensure a saturated coverage of PATP, i.e., formation of a complete self-assembled film of PATP. Then, the products were collected and rinsed thoroughly with ethanol, followed by redispersing in ethanol by sonication. Finally, one drop of the suspension was dropped onto the surface of a silicon wafer and dried in an atmosphere of nitrogen. For comparison purposes, Au nanoparticles ∼50 nm in diameter were prepared as the reference sample by reduction of $HAuCl_4$ (0.4 mM) with ascorbic acid (6 mM) in aqueous solution at room temperature.

Results and Discussion

Au Nanobelts Obtained at 4 °C. Figure 1a and b shows representative SEM and TEM images of the gold product obtained at 4 °C, which suggest that the product exclusively consists of very flexible, 1D belt-like nanostructures typically several tens of micrometers in length, ranging from 40 to 150 nm in width, and about 15−20 nm in thickness. The XRD pattern (Figure 2a) exhibits reflections characteristic of face-centered cubic (fcc) Au (Joint Committee on Powder Diffraction Standards (JCPDS) No. 04-0784), and the related energy-dispersive X-ray spectroscopy (EDS) spectrum (Figure S1) confirms that the nanobelts are composed of pure gold. Figure 1c shows a typical TEM image of an individual nanobelt as well as the related electron diffraction (ED) pattern, which can be indexed to the $[\bar{1}11]$ zone axis of gold, indicating that the whole Au nanobelt is a single crystal grown along the [110] direction and enclosed by the $(\bar{1}11)$ and $(\bar{1}12)$ planes as the top and side surfaces, respectively (Figure 1e). For simplicity, the obtained gold nanobelts with a cubic structure can be described as <110>-oriented with the {111} and {211} planes as the top and side surfaces, respectively, since <110> denotes a family of directions that are equivalent by the symmetry (e.g., [110], [101], [011], $[\bar{1}10]$, $[1\bar{1}0]$, $[\bar{1}\bar{1}0]$, etc.) and {211} denotes a set of face planes that are equivalent by the symmetry (e.g., (211), (121), (112), $(\bar{2}11)$, $(12\bar{1})$, $(1\bar{1}2)$, etc.). The HRTEM image shown in Figure 1d exhibits clear fringes with a spacing of ∼0.24 nm, which agrees well with the 3×{422} superlattice spacing of Au crystal,[22] confirming that the nanobelt is a single crystal grown along the <110> direction

(15) (a) Zhong, C. J.; Maye, M. M. *Adv. Mater.* **2001**, *13*, 1507. (b) Maye, M. M.; Luo, J.; Lin, Y. H.; Engelhard, M. H.; Hepel, M.; Zhong, C. J. *Langmuir* **2003**, *19*, 125. (c) Zhang, J. T.; Liu, P. P.; Ma, H. Y.; Ding, Y. *J. Phys. Chem. C* **2007**, *111*, 10382.

(16) (a) Borkowska, Z.; Tymosiak-Zielinska, A.; Shull, G. *Electrochim. Acta* **2004**, *49*, 1209. (b) Assiongbon, K. A.; Roy, D. *Surf. Sci.* **2005**, *594*, 99.

(17) Jena, B. K.; Raj, C. R. *J. Phys. Chem. C* **2007**, *111*, 15146.

(18) Narayanan, R.; El-Sayed, M. A. *J. Phys. Chem. B* **2005**, *109*, 12663.

(19) Fleischmann, M.; Hendra, P.; McQuilan, A. *Chem. Phys. Lett.* **1974**, *26*, 163.

(20) (a) Hu, X.; Cheng, W.; Wang, T.; Wang, Y.; Wang, E.; Dong, S. *J. Phys. Chem. B* **2005**, *109*, 19385. (b) Wang, T.; Zheng, R.; Hu, X.; Zhang, L.; Dong, S. *J. Phys. Chem. B* **2006**, *110*, 14179. (c) Wang, T.; Hu, X.; Dong, S. *J. Phys. Chem. B* **2006**, *110*, 16930.

(21) (a) Suzuki, M.; Niidome, Y.; Kuwahara, Y.; Terasaki, N.; Inoue, K.; Yamada, S. *J. Phys. Chem. B* **2004**, *108*, 11660. (b) Orendorff, C. J.; Gole, A.; Sau, T. K.; Murphy, C. *J. Anal. Chem.* **2005**, *77*, 3261.

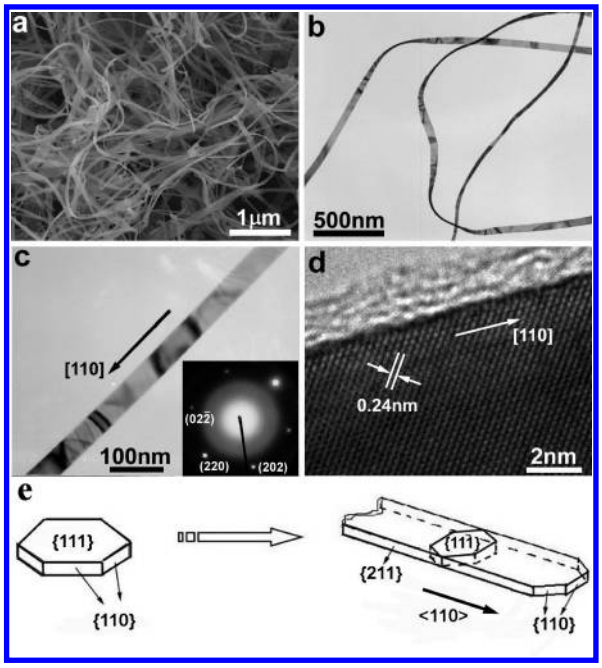

Figure 1. SEM (a), TEM (b,c), and HRTEM (d) images of gold nanobelts obtained at 4 °C. (e) Schematic illustration of the growth direction of gold nanobelts. (Inset) ED pattern corresponding to the whole region of c.

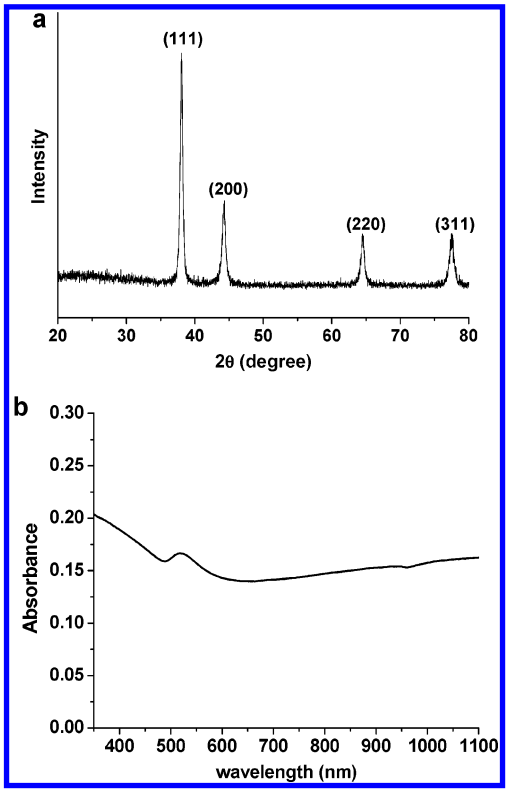

Figure 2. XRD pattern (a) and UV−vis absorption spectrum (b) of gold nanobelts obtained at 4 °C.

with the top surface of the {111} plane. Figure 1e presents a schematic illustration of the growth direction of the obtained <110>-oriented gold nanobelts, where a {111}-oriented hexagonal plate exhibiting 6 equivalent {110} planes as the side faces is drawn to more clearly show the relative angles between different planes and growth direction.

It is known that anisotropic gold nanoparticles normally exhibit two principle surface plasmon resonance (SPR) absorption peaks characteristic of the short (transverse band) and long (longitudinal band) axes.[2b] The absorption spectrum of the gold nanobelts suspended in water (Figure 2b) shows a peak around 520 nm due to the transverse plasmon band and an absorption increasing into the near-IR region without indication of leveling off, which could be attributed to the longitudinal plasmon band.[11] It is well known that the position and intensity of the longitudinal band depend largely on the size and aspect ratio of gold nanocrystals.[2] Notably, the SPR absorption due to the longitudinal plasmon band is not apparent, although an absorption increase can be observed in the near-IR region. This result could be attributed to the polydispersity in the length, width, and thickness of the nanobelts, which may lead to a variety of aspect ratios. The nonuniformity in the aspect ratio of the nanobelts could result in a longitudinal plasmon band with the position lying in a wide range of wavelengths, and the observed absorption spectrum may represent a contour combining the absorption spectra of gold nanobelts with varied aspect ratios. The partial overlapping between the transverse band and the longitudinal band could also lead to the apparently weak intensity of the SPR bands.

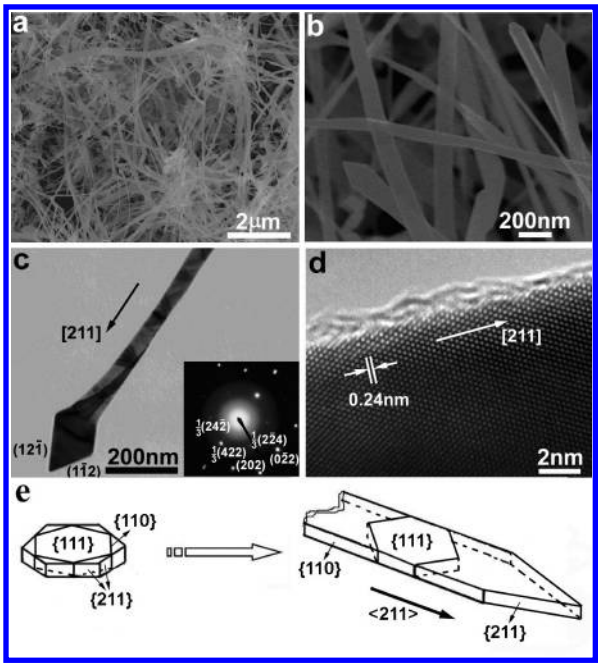

Figure 3. SEM (a,b), TEM (c), and HRTEM (d) images of gold nanobelts obtained at 27 °C. (e) Schematic illustration of the growth direction of the gold nanobelts. (Inset) ED pattern corresponding to the whole region of c.

Au Nanobelts Obtained at 27 °C. While the <110> direction is the predominant growth direction for the gold nanobelts obtained at 4 °C, the <211> direction turns out to be the exclusive growth direction for the gold nanobelts obtained at 27 °C. As shown in Figure 3a and b, nested gold nanobelts typically several tens of micrometers in length, ranging from 40 to 200 nm in width, and about 20−30 nm in thickness were produced. It can be noted that most of the nanobelts emanated from certain knots and ended with a triangular corner ~60°. Figure 3c presents a typical TEM image of an individual nanobelt as well as the related ED pattern showing the forbidden (1/3){422} reflection, which can be indexed to the [$\bar{1}$11] zone axis of gold, indicating that the whole Au nanobelt is a single crystal grown along the [211] direction with the (111) plane as the top surface. It is noteworthy that the nanobelt is enclosed by the {110} and {211} planes as the side surface for the straight central part and the diamond-like triangular end, respectively. The HRTEM image

(22) Kan, C.; Zhu, X.; Wang, G. *J. Phys. Chem. B* **2006**, *110*, 4651.

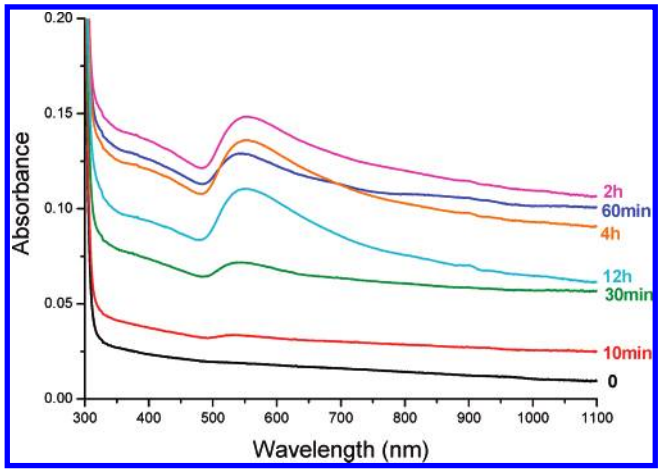

Figure 4. UV−vis absorption spectra of the gold products obtained at 27 °C at different reaction times.

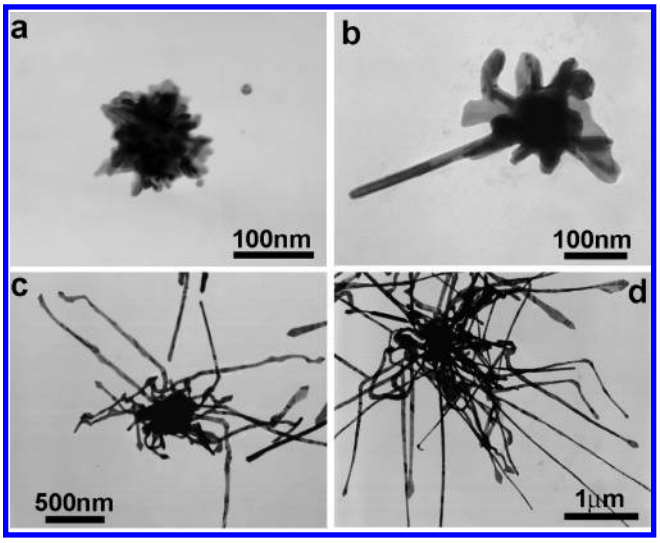

Figure 5. TEM images of gold products obtained at early stages of the gold nanobelts formed at 27 °C: (a) 15, (b) 30, and (c,d) 60 min.

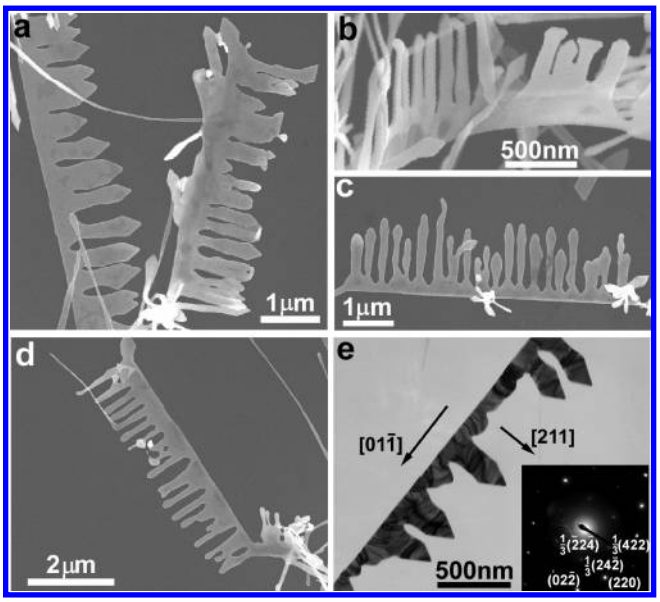

Figure 6. SEM (a−d) and TEM (e) images of gold nanocombs obtained by a two-step process with temperature changing from 4 to 27 °C. (Inset) ED pattern corresponding to the whole region of e.

shown in Figure 3d exhibits clear fringes attributed to the 3×-{422} superlattice spacing of Au crystal, confirming that the nanobelt is a single crystal grown along the <211> direction with the top surface of the {111} plane. Figure 3e presents a schematic illustration of the growth direction of the obtained <211>-oriented gold nanobelts, where a {111}-oriented hexagonal plate is drawn to more clearly show the relative angles between different planes and growth direction. Interestingly, while the <110>-oriented Au nanobelts are usually flexible with irregular ends, most of the <211> -oriented Au nanobelts are relatively rigid with triangular ends and some have side branches grown still along the <211> directions with a deviating angle of 60° (Figure S2).

Progress of the formation of the gold nanobelts obtained at 27 °C was followed by the in situ measurement of the UV−vis spectra. The reaction solution containing CTAB, SDSn, $HAuCl_4$, and ascorbic acid was introduced into a quartz cell thermostated at 27 °C immediately after mixing, and the UV−vis spectra were recorded at different time intervals. The color of the solution changed gradually from colorless to light pink within 15 min after mixing. Figure 4 shows the time-dependent spectral response obtained during the growth of Au nanobelts. The spectra recorded in the early stage (up to 60 min) show a broad peak at ∼540 nm, which can be assigned to the transverse component of SPR absorption. The intensity of the peak increases monotonically with time, indicating the increase in the amount of the gold products. The representative TEM images of the gold products obtained at the early stages of the nanobelt formation are presented in Figure 5. After 15 min of mixing, thorny nanoparticles of about 100 nm were produced as nuclei and short nanobelts emanated from these nuclei to form branched nanoparticles at 30 min. After 60 min of reaction, the short nanobelts grew into long nanobelts with different lengths, i.e., nested nanobelts with different overall sizes were produced, which finally evolved into the nested nanobelts shown in Figure 3. It can be observed from Figure 4 that the intensity of the UV−vis absorption peak increases up to 2 h, and then it decreases monotonically because of the gradual sedimentation of the large aggregates of nested nanobelts in the quartz cell. It is noted that the SPR absorption due to the longitudinal plasmon band cannot be observed throughout the growth process of the nanobelts, although a long absorption tail in the near-IR region is evident. This result could be attributed to the polydispersity in the length, width, and thickness of the nanobelts, similar to the situation of the gold nanobelts obtained at 4 °C.

Au Nanocombs Obtained by a Two-Step Process. When the reaction solution was initially kept at 4 °C for 0.5 h and subsequently let to stand at 27 °C for 12 h, unique gold nanocombs made of nanobelts about 20−30 nm in thickness could be obtained in addition to the nested Au nanobelts (Figure 6). The obtained comb-like nanostructures normally consist of a stem belt typically 3−10 μm in length and numerous lateral belts grown perpendicularly on one side of the stem. The ED pattern of a single nanocomb (Figure 6e) suggests that the gold nanocomb is actually a single crystal with the stem nanobelt grown along the <110> direction and the side nanobelts grown along the <211> direction, which are consistent with the growth directions of Au nanobelts grown at 4 and 27 °C, respectively. Note that for cubic gold, the [110] direction is equivalent to the [01$\bar{1}$] direction by the symmetry, and they can be simply unified as the <110> direction. Occasionally, lateral belts grew on the stem with an angle of 30° (e.g., the top end of the right comb in Figure 6a and the top end of the comb in Figure 6d), which still corresponded to the <211> growth direction. To our knowledge, it is for the first time that

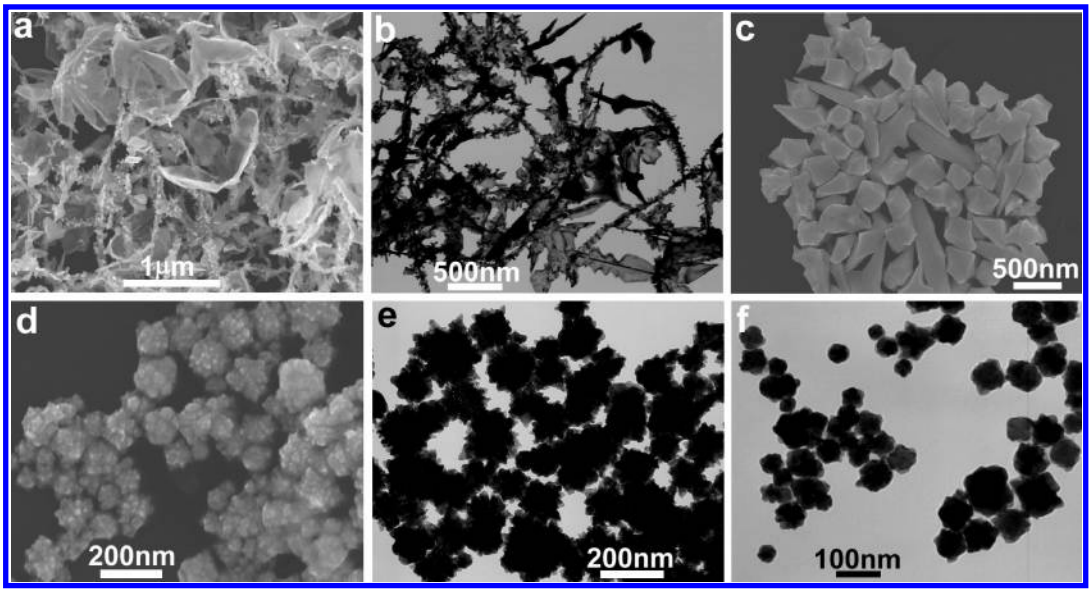

Figure 7. SEM (a,c,d) and TEM (b,e,f) images of gold nanostructures obtained at 4 (a,b,d,e) and 27 °C (c,f) in aqueous solutions of single surfactant: (a−c) 6.5 mM CTAB and (d−f) 1.0 mM SDSn.

such belt-based, comb-like nanostructures were synthesized for metal crystals with a cubic structure, although nanocombs or nanosaws were reported for ZnO,[23] ZnS,[24] and CdSe[25] crystals with a hexagonal structure.

Growth Mechanism. It was found that the presence of the CTAB−SDSn mixture was essential for formation of the gold nanobelt-based nanostructures. When CTAB was used as the single surfactant, wire-like and leaf-like particles were obtained at 4 °C whereas irregular polyhedral particles were obtained at 27 °C under similar synthesis conditions; on the other hand, irregular star-like particles were produced at either 4 or 27 °C when SDSn was used as the single surfactant (Figure 7). The exact formation mechanism of the gold nanobelts grown at two different directions at 4 and 27 °C remains to be elucidated; however, we believe that the mixed surfactants could play the role of binary capping agents for nanobelt growth and the change of temperature would exert a subtle influence over the capping process and thus induce the change in the growth direction. It has been shown that mixed cationic−anionic surfactants may interact with inorganic nanocrystals in a synergistic way and adsorb on specific crystal surfaces in the form of a mixed surfactant film.[26] In particular, the packing state of the interfacial mixed film, which can be significantly affected by various parameters such as the temperature and mixing ratio of the mixed surfactants, would largely influence the specific adsorption of the mixed surfactants on the growing nanocrystals.[27] In addition, the temperature would significantly influence the aggregation state of mixed surfactants in solution; for example, the sizes of the aggregates were apparently decreased with increasing temperature, which might affect the specific adsorption of the mixed surfactants on the surfaces of gold nanocrystals.

On the basis of the above experimental results, a tentative growth mechanism for the gold nanobelts and nanocombs is illustrated in Figure 8. The CTAB−SDSn mixture could strongly

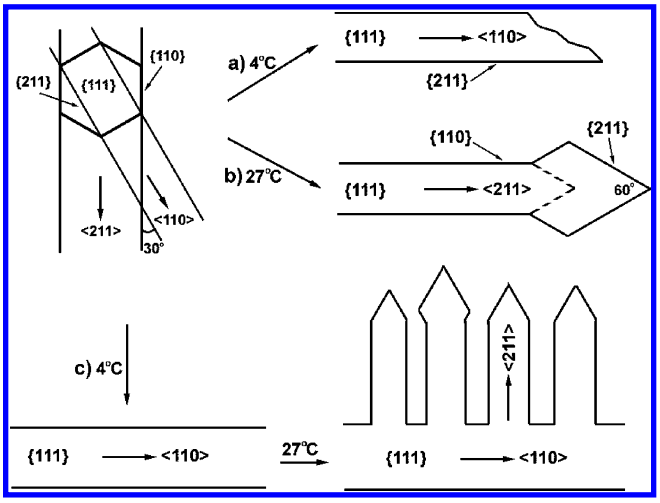

Figure 8. Schematic illustration of the formation mechanism of gold nanobelts and nanocombs. In the upper left corner is presented a projection perpendicular to the top surface of the {111} plane including a hexagonal prism to show the relative angles between different growth directions and side faces of the two kinds of nanobelts.

adsorb on the {111} planes of cubic gold at both temperatures; meanwhile, it could less strongly adsorb on the {211} surfaces at 4 °C and on the {110} surfaces at 27 °C, leading to formation of <110>-oriented nanobelts and <211>-oriented nanobelts at 4 and 27 °C, respectively. The growth of gold nanocombs via a two-step process with temperature changing from 4 to 27 °C could be rationalized by considering that the <110>-oriented stem nanobelts formed at 4 °C initially, which was followed by the gradual growth of <211>-oriented lateral nanobelts on one side of the stem. The proposed formation mechanism of the gold nanocombs was supported by our preliminary investigation on early stages of the gold nanocombs. As shown in Figure 9a, toothed nanobelts appeared when the nanobelts formed after 30 min of aging at 4 °C were further aged at 27 °C for 10 min. Furthermore, the ED pattern of a single toothed nanobelt (Figure 9b) suggests that it is actually a single crystal with the stem nanobelt grown along the <110> direction and the tooth grown along the <211> direction, which is consistent with the growth directions of the final gold nanocombs shown in Figure 6. The

(23) (a) Wang, Z. L.; Kong, X. Y.; Zuo, J. M. *Phys. Rev. Lett.* **2003**, *91*, 185502. (b) Wang, J. X.; Sun, X. W.; Wei, A.; Lei, Y.; Cai, X. P.; Li, C. M.; Dong, Z. L. *Appl. Phys. Lett.* **2006**, *88*, 233106. (c) Li, Y.; Zou, K.; Shan, Y. Y.; Zapien, J. A.; Lee, S.-T. *J. Phys. Chem. B* **2006**, *110*, 6759.
(24) Ma, C.; Moore, D.; Li, J.; Wang, Z. L. *Adv. Mater.* **2003**, *15*, 228.
(25) Ma, C.; Ding, Y.; Moore, D.; Wang, X.; Wang, Z. L. *J. Am. Chem. Soc.* **2004**, *126*, 708.
(26) Shi, H.; Qi, L.; Ma, J.; Cheng, H.; Zhu, B. *Adv. Mater.* **2003**, *15*, 1647.
(27) Shi, H.; Qi, L.; Ma, J.; Wu, N. *Adv. Funct. Mater.* **2005**, *15*, 442.

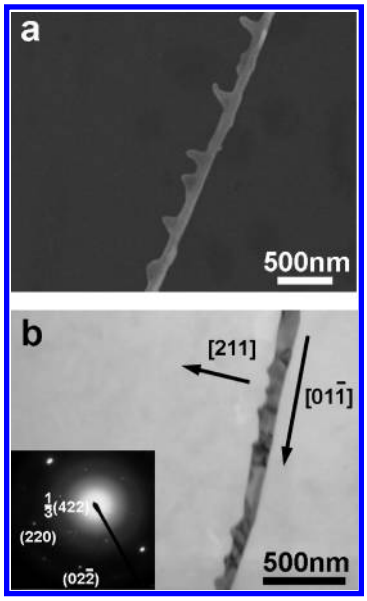

Figure 9. SEM (a) and TEM (b) images of toothed gold nanobelts obtained after reacting at 4 °C for 30 min and then 10 min at 27 °C. (Inset) ED pattern corresponding to the whole region of b.

reason why the lateral nanobelts of the nanocombs just grow along one side (e.g., grow along the [211] direction but not along the [2$\bar{1}$1] direction simultaneously) remains unclear. A possible explanation could be that one side of the stem nanobelt was tightly adsorbed by the mixed surfactants or approached by the aggregates of the mixed surfactants during the gradual growth of lateral nanobelts on the other side. Such a breaking of symmetry in the crystal growth represents an interesting topic worthy of further study. Furthermore, a detailed investigation on the effects of the temperature and mixing ratio of the cationic/anionic surfactants on the growth processes of the gold nanostructures is needed to fully elucidate the growth mechanism of the gold nanobelts and nanocombs, which is currently underway in our lab.

Electrocatalysis. The freshly prepared gold nanobelts-modified GC electrodes and a clean poly crystalline Au (abbreviated to poly-Au) electrode were characterized in alkaline solutions by means of cyclic voltammetry to compare the electrochemical properties between gold nanobelts and poly-Au. Hereafter, the GC electrodes modified with gold nanobelts obtained at 27 and 4 °C are denoted as 27 °C gold nanobelts electrode and 4 °C gold nanobelts electrode, respectively. It was found that the structure of the nanobelts on the electrode surface was basically retained after continuous potential cycling. The surface area of the gold nanobelts was measured by cyclic voltammetry using the $Fe(CN)_6^{3-/4-}$ redox couple, and the calculated surface area for the 27 and 4 °C gold nanobelts electrode was 0.0354 and 0.0428 cm^2, respectively. Figure 10a shows the cyclic voltammograms (CVs) obtained for the gold nanobelts modified GC electrodes and poly-Au electrode in 0.1 M KOH in the potential range from −0.1 V to 0.65 V. A broad oxidation wave and a reduction peak are observed for all three kinds of modified electrodes. The oxidation peak can be ascribed to formation of gold surface oxides, and the reduction peak can be ascribed to subsequent removal of the oxides. As compared with the voltammetric behavior of the poly-Au electrode, the oxidation peaks of the gold nanobelts electrodes occur at less positive potentials. Moreover, the peak current for gold surface oxides at the gold nanobelts electrodes is significantly higher than that at poly-Au electrode. For comparison of the electrocatalytic activity between gold nanobelts and poly-Au, the current was normalized with the

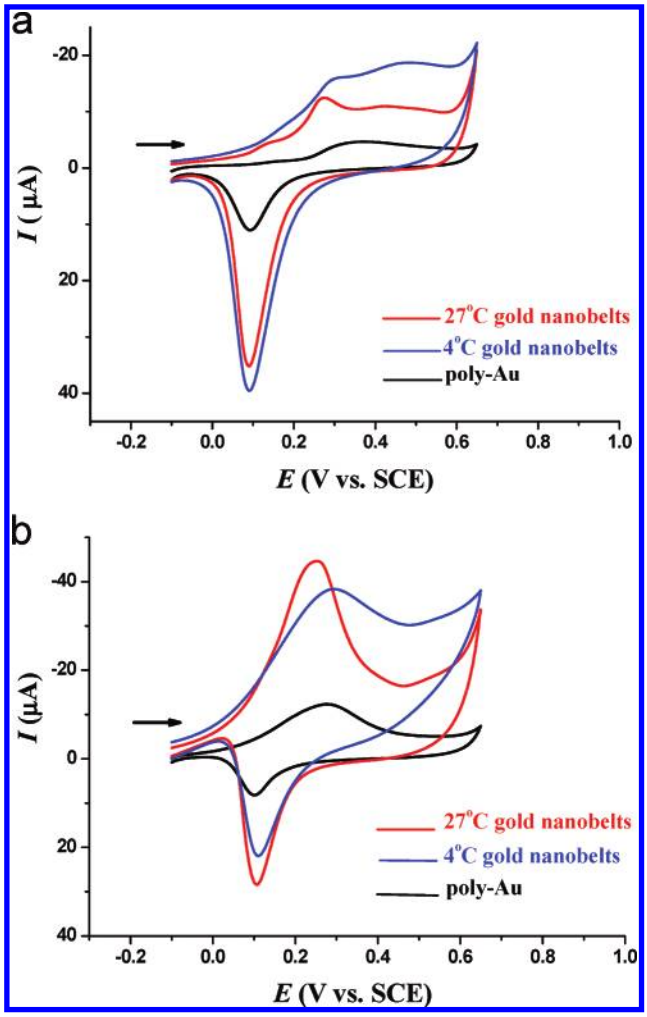

Figure 10. Cyclic voltammograms of gold nanobelt electrodes and polycrystalline Au (poly-Au) electrode in 0.1 mol dm^{-3} KOH solutions in the absence (a) and presence (b) of 1.0 mol dm^{-3} CH_3-OH. The potential scan rate was 10 mV s^{-1}.

surface area to obtain the current density. It was found that the current densities obtained at the gold nanobelts electrodes were much higher than that at poly-gold electrode , indicating that the gold nanobelts were oxidized more readily than poly-Au under otherwise identical conditions. In addition, the gold nanobelts obtained at 27 °C were oxidized more readily than the gold nanobelts obtained at 4 °C.

The electrocatalytic activity of gold nanobelts toward the oxidation of methanol was investigated by measuring the CVs of the gold nanobelts electrodes in the alkaline solution containing methanol. Figure 10b displays the typical CVs of the gold nanobelts electrodes and the normal poly-Au electrodes, which were electrochemically activated by treating with vitriol, in 0.1 mol dm^{-3} KOH solution with 1.0 mol dm^{-3} CH_3OH. The CVs of all the three gold electrodes clearly show that methanol oxidation occurs in a potential region from −0.2 to 0.40 V (vs SCE), which may be ascribed to oxidation of methanol to formates via a four-electron-transfer reaction.[16a,28] Compared with the CVs of the gold nanobelts electrodes in methanol-free solution (Figure 11a), there is not a sharp increase of the anodic current for methanol oxidation at potentials higher than 0.5 V, which means that methanol is not further oxidized to carbonates in the present

(28) Tremiliosi-Filho, G.; Gonzalez, E. R.; Motheo, A. J.; Belgsir, E. M.; Leger, J.-M.; Lamy, C. *J. Electroanal. Chem.* **1998**, *444*, 31.

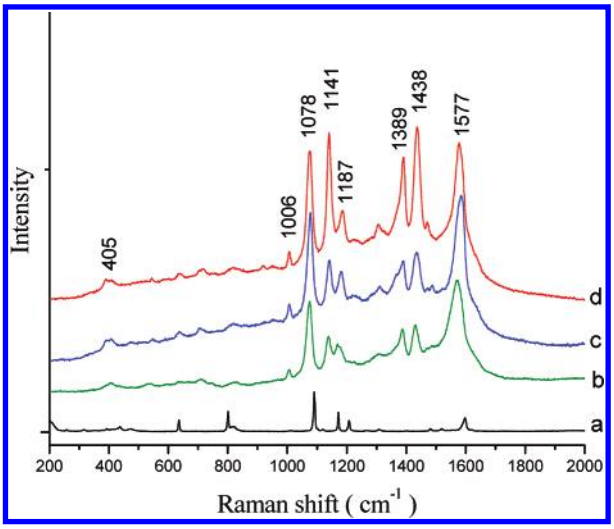

Figure 11. Raman spectrum of solid PATP (a), and SERS spectra of PATP molecules adsorbed on different substrates: (b) ~50 nm gold nanoparticles; (c) gold nanobelts obtained at 27 °C; (d) gold nanobelts obtained at 4 °C.

case. It is known that electrooxidation of methanol depends on the preoxidation species of gold, such as $Au-OH_{ads}^{(1-\lambda)-}$, where "ads" denotes the chemisorbed species on gold and the charge-transfer coefficient λ varies between 0 and 1.[15c,16b] When the preoxidation species are consumed to form gold oxides, the methanol oxidation reaction will be slowed down and stopped;[15c] therefore, methanol electrooxidation takes place in the potential region between −0.2 and 0.40 V. It can be seen from Figure 10b that the poly-Au electrode shows an oxidation peak at a more positive potential (0.275 V) compared with the oxidation peak for the 27 °C gold nanobelts electrode (0.25 V). Moreover, the current density calculated for the oxidation of methanol at the 27 °C gold nanobelts electrode is significantly higher than that at poly-Au electrode, indicating that the freshly prepared 27 °C gold nanobelts electrode has higher electrocatalytic activity than the electrochemically activated poly-Au electrode. The high electrocatalytic activity could be ascribed to the special morphology of nested gold nanobelts, which is reminiscent of the high electrocatalytic activity toward methanol oxidation observed from gold nanoflowers electrodes.[9e] The 4 °C gold nanobelts electrode shows an oxidation peak at ~0.28 V with a current density somewhat less than that at the 27 °C gold nanobelts electrode. The relatively lower electrocatalytic activity compared to the 27 °C gold nanobelts may be rationalized by considering that the 4 °C gold nanobelts are much softer and longer than the 27 °C gold nanobelts, and hence, they tend to form rather compact aggregates on the electrode.

The effects of the methanol concentration and scan rate on the CV curves for oxidation of methanol on 27 °C gold nanobelts electrode were examined (Figure S3). As shown in Figure S3a, the cathodic peak corresponding to reduction of surface oxide decreases with increasing methanol concentration, which confirms the involvement of surface oxides in the catalytic reaction.[9e] On the other side, oxidation of methanol reinitiates with the removal of the gold surface oxides, and a corresponding oxidation current regains after the potential reaches ~0.1 V. Both the cathodic peak current (i_{pc}) and the anodic peak current (i_{pa}) increase with the increase of the scan rate. The i_{pa} is approximately linear with $v^{1/2}$ when $v > 20$ mV s^{-1} (Figure S3b). The ratio between i_{pa} and i_{pc} decreases with increasing v, indicating a surface redox-mediated catalytic oxidation.[29] It has been found that the electrocatalytic activity of the gold nanobelt electrode is very stable upon repetitive cycling in the potential window used, indicating that the gold nanobelts are free from the poisoning effect.

SERS Measurements. To investigate the SERS sensitivity of the gold nanobelts substrates, the Raman spectra of the PATP molecules adsorbed on the surface of gold nanobelts as well as normal gold nanoparticles ~50 nm in diameter (Figure S4), which were prepared by simply reducing $HAuCl_4$ with ascorbic acid in aqueous solution, were measured. Compared with the normal Raman spectrum of solid PATP (Figure 11a), noticeable changes in the frequency shift and relative intensity of the bands can be observed from the SERS spectra on different gold substrates, indicating that the thiol group in PATP directly contacts with the gold surfaces.[20c,30] The SERS spectra obtained from ~50 nm gold nanoparticles (Figure 11b) and the 27 °C gold nanobelts (Figure 11c) are dominated with the a_1 vibrational modes (in-plane, in-phase modes), such as ν(CC) and ν(CS) at 1577 and 1078 cm^{-1} for the 27 °C gold nanobelts. The predominance of a_1 modes in the SERS spectra may imply that the enhancement via an electromagnetic (EM) mechanism is significant.[19] However, the enhancement of b_2 modes (in-plane, out-of-phase modes) located at 1438, 1389, 1141, 1187, and 1006 cm^{-1} is also apparent. The apparent enhancement of b_2 modes may be ascribed to the charge transfer (CT) of the metal to the adsorbed molecules, which demonstrates that the PATP molecules contact with the gold surface by forming a strong Au−S bond.[20b,c]

Interestingly, the SERS spectrum obtained from the 4 °C gold nanobelts is dominated by the bands at 1438 and 1141 cm^{-1} (Figure 11d), suggesting that the b_2 modes gain larger enhancement than a_1 modes. This result is unusual for the SERS measurement from pure gold substrate, although the SERS spectra with dominant b_2 modes were previously obtained from assemblies of Au(core)/Cu(shell) nanoparticles.[31] It has been suggested that the enhancement of the b_2 modes of the PATP molecules is largely dependent on the supporting substrate and the assembly structure of the metal nanoparticles.[32] For example, larger enhancement of the b_2 modes relative to that of the a_1 modes was reported for the two-dimensional arrays of submicrometer silver cavities, which was attributed to the charge transfer induced by the assembled nanoparticles.[32] Compared with the 27 °C gold nanobelts, which are ~20−30 nm in thickness and <211>-oriented with {110} side surfaces, the 4 °C nanobelts are relatively thinner (~15−20 nm) and have a different growth direction, i.e., <110>-oriented with {211} side surfaces. It has been documented that the different facets of gold with different surface energies could result in the different enhancement effects in SERS measurements; for example, greater Raman enhancement is observed for PATP molecules on Au{110} than Au{111} due to the higher surface energy of Au{110}.[33] Therefore, it may be reasonably speculated that the difference in the exposed side facets of the gold nanobelts would largely contribute to the unusual enhancement of the b_2 modes in the SERS spectrum obtained from the 4 °C nanobelts. In addition, the Raman enhancement could also be influenced by the thickness of the nanobelt as well as the aggregation state of the gold nanobelts assembled on the

(29) Lou, Y.; Maye, M. M.; Han, L.; Luo, J.; Zhong, C. *J. Chem. Commun.* **2001**, 473.
(30) (30) Wei, G.; Wang, L.; Liu, Z.; Song, Y.; Sun, L.; Yang, Y.; Li. Z. *J. Phys. Chem. B* **2005**, *109*, 23941.
(31) Cao, L.; Diao, P.; Tong, L.; Zhu, T.; Liu, Z. *Chem. Phys. Chem.* **2005**, *6*, 913.
(32) Zhou, Q.; Zhao, H.; Pang, F.; Jing, Q.; Wu, Y.; Zheng, J. *J. Phys. Chem. C* **2007**, *111*, 514.
(33) (a) Nikoobakht, B.; Wang, J.; El-Sayed, M. A. *Chem. Phys. Lett.* **2002**, *366*, 17. (b) Hu, X.; Wang, T.; Wang, L.; Dong, S. *J. Phys. Chem. C* **2007**, *111*, 6962.

Si substrate. The observed interesting SERS properties of the gold nanobelts with different growth directions are worthy of further investigation.

Conclusions

Well-defined gold nanobelts grown along two different directions and unique gold nanocombs consisting of these two kinds of nanobelts were synthesized in aqueous solutions of mixed surfactants by simply controlling the reaction temperature. The mixed cationic−anionic surfactants exerted a subtle control on the growth of gold nanocrystals in solution due to the cooperative effect of mixed surfactants, which was advantageous over the simple control provided by single surfactants. This synthetic strategy may open a new route for the mild fabrication and hierarchical assembly of metal nanobelts in solution. Both the <211>-oriented gold nanobelts obtained at 27 °C and the <110>-oriented gold nanobelts obtained at 4 °C were used as electrode materials for the electrocatalytic oxidation of methanol and as the SERS substrate for detecting the enhanced Raman spectra of PATP molecules. While the nested gold nanobelts obtained at 27 °C show a much higher electrocatalytic activity than normal polycrystalline gold electrode, the <110>-oriented gold nanobelts obtained at 4 °C exhibited an unusual larger enhancement of the b_2 modes relative to the a_1 modes for the adsorbed PATP molecules. The obtained gold nanobelts and nanocombs would be ideal candidates for investigating the electrical properties of 1D metal nanostructures with specific growth direction and cross-sectional aspect ratio[34] as well as the novel photonic properties of hierarchical architectures of 1D metal nanostructures as potential plasmonic fibers.[35] Moreover, the unique gold nanocombs showing a cantilever-like structure could find promising applications in biosensing and nanodevices.[36,37]

Acknowledgment. This work was supported by the National Natural Science Foundation of China (20325312, 20673007, 20473003, and 20633010) and MOST (2007CB936201).

Supporting Information Available: EDS spectrum and further TEM characterization of the gold nanobelts as well as detailed cyclic voltammograms for the methanol oxidation catalyzed by the gold nanobelts. This information is available free of charge via the Internet at http://pubs.acs.org.

LA702848X

(34) Wiley, B. J.; Wang, Z.; Wei, J.; Yin, Y.; Cobden, D. H.; Xia, Y. *Nano Lett.* **2006**, *6*, 2273.
(35) Sanders, A. W.; Routenberg, D. A.; Wiley, B. J.; Xia, Y.; Dufresne, E. R.; Reed, M. A. *Nano Lett.* **2006**, *6*, 1822.
(36) Ferrari, M. *Nat. Rev. Cancer* **2005**, *5*, 161.
(37) Watari, M.; Galbraith, J.; Lang, H.-P.; Sousa, M.; Hegner, M.; Gerber, C.; Horton, M. A.; McKendry, R. A. *J. Am. Chem. Soc.* **2007**, *129*, 601.